Hybrid Plasmonics and Two-Dimensional Materials: Theory and Applications

Article *in* Journal of Molecular and Engineering Materials · July 2020

DOI: 10.1142/S2251237320300016

9 authors, including:

Matěj Šebek
University College London
22 PUBLICATIONS **84** CITATIONS
SEE PROFILE

Ahmed Elbanna
Nanyang Technological University
8 PUBLICATIONS **87** CITATIONS
SEE PROFILE

Arash Nemati
Advanced Science Research Center, GC/CUNY
16 PUBLICATIONS **385** CITATIONS
SEE PROFILE

Xiaodi Su
Institute of materials research and engineering
136 PUBLICATIONS **5,592** CITATIONS
SEE PROFILE

Hybrid Plasmonics and Two-Dimensional Materials: Theory and Applications

Matej Sebek[1,2], Ahmed Elbana[1,3], Arash Nemati[1,4], Jisheng Pan[1], Ze Xiang Shen[3], Minghui Hong[4], Xiaodi Su[1], Nguyen Thi Kim Thanh[2,5*], Jinghua Teng[1*]

[1] *Institute of Material Research and Engineering, Agency for Science, Technology and Research, Singapore*
[2] *Department of Physics and Astronomy, University College London, London, United Kingdom*
[3] *School of Physical and Mathematical Sciences, Nanyang Technological University, Singapore*
[4] *Department of Electrical and Computer Engineering, National University of Singapore, Singapore*
[5] *UCL Healthcare and Nanomaterials Laboratory, London, United Kingdom*

The inherent thinness of 2D materials limits their efficiency of light-matter interactions and high loss of noble metal plasmonic nanostructures limits their applicability. Thus a combination of 2D materials and plasmonics is highly attractive. This review describes the progress in the field of 2D plasmonics, which encompasses 2D plasmonic materials and hybrid plasmonic-2D materials structures. Novel plasmonic 2D materials, plasmon-exciton interaction within 2D materials and applications comprising sensors, photodetectors and, metasurfaces are discussed.

Keywords: 2D materials, plasmonics, 2D plasmons, plasmon-exciton interaction, plasmon-enhanced photoluminescence, SPR biosensors, photodetectors

1. Introduction

Surface plasmon polaritons comprised of thin metal films are commonly used for Surface Plasmon Resonance (SPR) sensors,[1] for the detection of a variety of analytes ranging from gases[2] to the SARS-CoV-2 virus[3]. Plasmonic nanostructures are widely used due to the subwavelength confinement of electromagnetic field and wide variability of tunability of the resonance response by geometrical tailoring.[4] They have found their applications in sensing[5–7], bioimaging[8–11], photothermal[8] and photodynamic therapy[12], drug delivery[11;13;14], metamaterials[15;16], nanolasers[17], stable colours,[18], and for surface enhanced Raman Scattering (SERS).[19] The subwavelength confinement of light also allows lithography[20;21] and nano-imaging[22] with sub-diffraction limited resolution.

Since the discovery of graphene[23], two dimensional (2D) materials have attracted tremendous attentions for a range of interesting properties including strong light-matter interaction[24;25], exceptional carrier mobilities[26;27], and the possibility to tailor the electronic and optical properties by an assembly of layered heterostructures.[28] In recent years, 2D semiconductors are of special interest since MoS_2 was revealed to be a direct band-gap semiconductor.[29] Heterostructures of 2D semiconductors may exhibit long-lived interlayer excitons[30] with controllable energy, polarization[31] and spatial distribution[32]. Properties of 2D semiconductors are also controllable by carrier injection using 2D metals such as graphene.[33] Stacking graphene with 2D semiconductors while using hexagonal boronitride (hBN) as a 2D insulator allows the development of all-2D transistors.[34;35] In recent years, light emitting devices (LEDs)[36;37], lasers[38;39], photodetectors[40;41] and photovoltaic devices[42] based on 2D materials have been demonstrated.

However, the inherent thinness of the materials limits the efficiency of light-matter interactions and hinders the possibility for real-life applications. Also, high loss of noble metal plasmonic nanostructures limits their applicability

for optical circuitry.[43] That makes the connection of plasmonics and 2D materials either in the form of 2D plasmonic material or the form of hybrid plasmonic 2D material structure highly attractive.[44] The former such as graphene is plasmonic material in mid to far infrared range which offers extraordinary light confinement[45] and possesses much lower loss than noble metals[46], while the latter enhances the light-matter interactions within the 2D materials by strong field confinement offered by plasmonic nanostructures.[47]

Here, we present a review on plasmonics with 2D materials in both fundamentals and potential applications. After a brief introduction to plasmonics, we'll have a look at plasmonics within 2D materials including the well-known graphene, other 2D metallic and doped semiconducting materials as well as 2D noble metals. Attention is then turned to the interactions of plasmonic structure with 2D materials especially transition metal dichalcogenides (TMDC). The last section is dedicated to the emerging applications followed by a brief contemplation on the possible future course of research in this field.

2. A brief introduction to plasmonics

2.1. *Surface plasmon polaritons*

Surface plasmon polaritons (SPPs) are transverse magnetic (TM) polarized electromagnetic waves coupled with collective oscillations of the electron cloud (plasmons) travelling along metal-dielectric interface. Their dispersion relation in the terms of wavenumber $k(\omega)$ is given by[48]:

$$k_x(\omega) = \frac{\omega}{c}\sqrt{\frac{\epsilon(\omega)\epsilon_D}{\epsilon(\omega)+\epsilon_D}}, \qquad (1)$$

where k_x is the x component of the wave vector parallel to the surface (see Fig. 1), ω is the frequency of the incident light, ϵ_D is the dielectric function of the dielectric and $\epsilon(\omega)$ the metal dielectric function derived from Drude model. Figure 1a shows how the surface plasmon polariton propagates along the metal/dielectric interface.[49]

Due to different dispersion and momentum mismatch, SPP normally cannot be excited by photons from free space. A prism or a grating is commonly used to modify the k of the incident light wave to couple with SPP.[50]

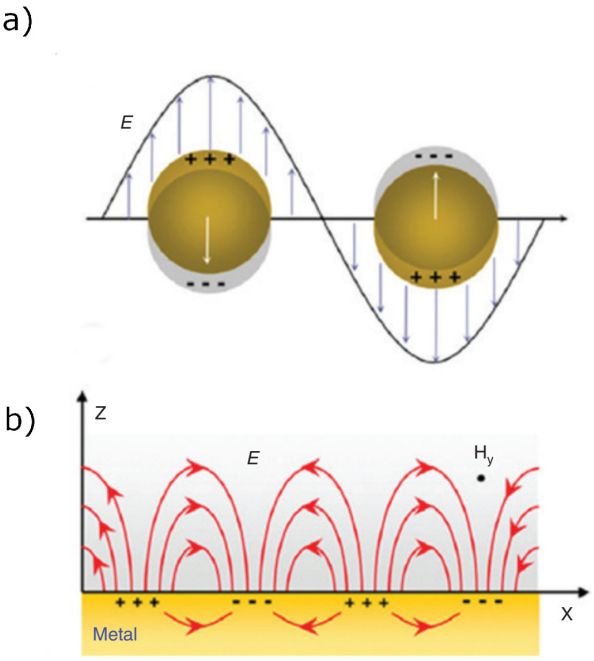

Fig. 1: a) Surface plasmon polariton propagating along metal/dielectric interface b) Localized surface plasmon polariton within a metal nanosphere. Reproduced from[49] with permission. Copyright 2017, MDPI.

2.2. *Localized surface plasmon polaritons*

The localized surface plasmon resonance (LSPR) is an effect occurring when the collective valence electron oscillation in a metal nanoparticle is in resonance with incident light. As a result of LSPR, the integral effect of the aforementioned electron oscillation causes the local enhancement of the electromagnetic field near the nanoparticle.[51]

The Mie theory gives the extinction spectrum E (λ) of the nanoparticle as[52]:

$$E(\lambda) = \frac{C\epsilon_{out}^{3/2}}{\lambda}\left[\frac{\epsilon_i(\lambda)}{(\epsilon_r(\lambda)+\xi\epsilon_{out})^2+\epsilon_i(\lambda)^2}\right], \qquad (2)$$

where λ is the wavelength of the incident light, C is a constant, ϵ_r and ϵ_i real and imaginary parts of the metal dielectric constant respectively, ϵ_{out} a dielectric constant of the surrounding media and ξ a shape factor of the nanoparticle (for example ξ for a sphere is 2). The dielectric resonance then

occurs when $\epsilon_r \approx \xi\epsilon_{out}$.

The real part of the dielectric function ϵ_r determines the plasmonic properties of the material and the condition for exciting the plasmon resonance requires ϵ_r to be negative. In a quasi-static approach, the localized surface plasmons depend linearly on dielectric function. In addition, the ohmic loss, described by the imaginary part of dielectric function ϵ_i, degrades the performance of the plasmonic device. The quality factor Q gives information about the performance of a particular material:

$$Q_{LSP} = -\frac{\epsilon_r}{\epsilon_i}. \tag{3}$$

The maximum value of the quality factor can be expressed by the Drude model as[53]:

$$Q_{LSP}^{max} = \frac{2(\omega_P^2 - \gamma^2)^{3/2}}{3\gamma\omega_P^2\sqrt{3}}, \tag{4}$$

where γ is the damping and ω_P the plasma frequency defined as $\omega_P = \sqrt{\frac{n_e e^2}{m^* \epsilon_0}}$ with n_e and m^* being the carrier charge density and effective electron mass respectively. Figure 1b shows the oscillation of the electron cloud inside of a nanoparticle excited by an electromagnetic wave.[54]

3. 2D plasmonic materials

3.1. *Graphene plasmons*

Plasmons in graphene are fundamentally different from those in noble metals.[45;55;56] The band structure of graphene consists of two Dirac cones (shown in Figure 2a) touching at a so-called Dirac point, which implies the linear dispersion of carriers.[57] The optical response of graphene in the local limit is described by the local Random Phase Approximation as:

$$\sigma(\omega) = -\frac{e^2}{\pi\hbar^2}\frac{i}{\omega + i\tau^{-1}}\int_{-\infty}^{\infty} dE \left[|E|\frac{\partial f_E}{\partial E} + \right. \\ \left. + \frac{(E/|E|)}{1 - 4E^2/[\hbar^2(\omega + i\tau^{-1})^2]} f_E\right], \tag{5}$$

where $\sigma(\omega)$ is the conductivity, ω is the frequency of the incident light, f_E the Fermi-Dirac distribution of electrons, and τ the relaxation time of the intraband processes. In the equation, the first term describes the intraband transition and the second term describes the interband transition. At zero temperature ($f_E = \sigma(E_F - E)$ with E_F being the graphene Fermi level), the term simplifies to the form of Drude conductivity.[45]

The dispersion relation of the plasmons can be then expressed as:

$$k_{SP} \approx \hbar^2/4e^2E_F(\epsilon + 1)\omega(\omega + i/\tau), \tag{6}$$

where k_{SP} is the surface plasmon wave number. The graphene plasmons are extraordinarily confined both in the in-plane and out-of-plane directions.[56] Plasmons in graphene were firstly revealed by Fei et al.[58] by using scattering-type Scanning Nearfield Optical Microscope (s-SNOM), which is shown on Figure 2b. An AFM tip illuminated by a tunable infrared CO_2 laser acts as a near-field probe. Their gate-tunable properties were shown using the same technique by two groups in 2012. By applying a gate voltage the amplitude and the wavelength of the plasmons in graphene can be altered and plasmons can be completely turned off.[61;62]

Besides tuning the plasmons by changing the Fermi energy through gating, graphene plasmons are also tunable through geometry change. Graphene nanoribbons are central to the field of graphene plasmonics as the plasmon energy E_P scales with the width of the nanoribbon D placed on an interface of materials with the permittivities of ϵ_1 and ϵ_2 as[45]:

$$E_P \approx 4e\sqrt{2E_F/[\pi D(\epsilon_1 + \epsilon_2)]}. \tag{7}$$

Moreover, edge plasmons were shown to possess an ultrahigh refractive index and extremely small mode volume compared to the metal plasmons. Different plasmonic modes of graphene are shown in Figure 2c.[59]

This design has been employed to develop a tunable terahertz metamaterial. Graphene nanoribbons gated with an ionic gel were found to absorb 13% at room temperature in the terahertz range tunable over a range from 3000 cm^{-1} to 9000 cm^{-1}.[63]

The capability of tuning plasmon properties in graphene makes it suitable for many applications ranging from nanoelectronics to biosensing. The mid-IR range of the graphene plasmons overlaps with the range encompassing molecular vibrations of complex biomolecules, which could be highly enhanced with graphene plasmon resonance.[64] Rodrigo et al.[60] reported a tunable mid-IR

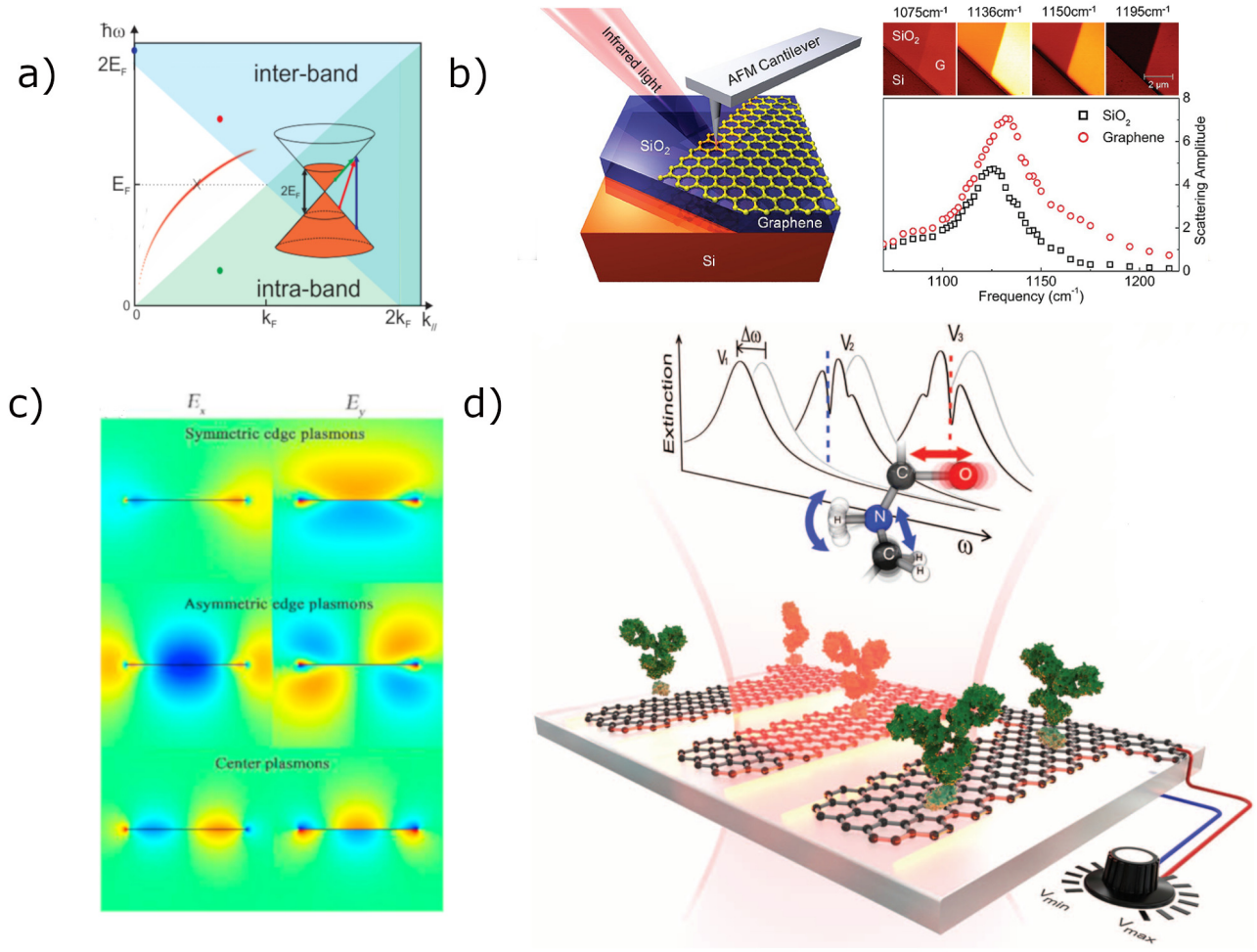

Fig. 2: a) The dispersion relation of the graphene plasmon, the inset shows the band structure of graphene with the characteristic Dirac cone. Reproduced from[56] with permission. Copyright 2011, American Chemical Society. b) Graphene plasmons imaged with s-SNOM. Reproduced from[58] with permission. Copyright 2011, American Chemical Society. c) Analytical calculation shows different plasmonic modes within graphene. Reproduced from[59] with permission. Copyright 2016, Elsevier. d) The schematic of a tunable graphene plasmonic biosensor with an mid-IR extinction of the tunable plasmon interacting with the biomolecule. Reproduced from[60] with permission. Copyright 2015, AAAS.

graphene-based biosensor (Figure 2d), in which the change of Fermi energy of graphene by applying a gate voltage shifts the graphene plasmon resonance. The sensor scans over a broad spectral range yielding a high sensitivity. From the response at different frequencies, the permittivity of the molecule can be reconstructed.

Recently, graphene plasmons have been theoretically proposed as a viable platform for quantum computing. It is a two-qubit logic gate with qubits encoded in graphene plasmons and most importantly, this technology would not require any cryogenic cooling.[65] The concept is based on an interaction between two graphene plasmons.[66;67]

3.2. *Two dimensional plasmonic materials beyond graphene*

3.2.1. *Novel 2D plasmonic materials*

In recent years, there have been efforts in looking for plasmonic materials beyond the widely used noble metals and graphene.[68;69] Bismuth telluride

- Bi_2Te_3 nanoplates have been shown to exhibit multiple plasmon modes covering the whole visible range. These modes in Bi_2Te_3 nanoplates result from spin-orbit coupling[70] and can have the plasmon resonance peak tuned by Se doping as much as 400 nm. Figure 3a shows an Elecron Energy Loss Spectroscopy (EELS) mapping of a single Bi_2Te_3 nanoplate.[71] Moreover, coupling Bi_2Te_3 with graphene enhances the plasmon excitation in graphene.[72]

Other interesting materials with plasmonic properties are 2D oxides of tungsten and molybdenum.[73] They can be ultra-doped and have also large dielectric constants. Importantly, the plasmon response of MoO_3 can be tuned by controlling oxygen vacancies. Simply by irradiating the material by sunlight in the presence of water, H^+ ions intercalate into the material and introduce oxygen deficiencies changing the colour dramatically and strengthening the plasmonic response, which can be seen in Figure 3b.[74] Such a material can be combined with metal nanoparticles to create a hybrid plasmonic structure.[75]

Highly doped 2D transition metal dichalcogenides such as MoS_2 exhibit surface plasmon resonances. That can be achieved by electrochemically intercalating bulk material and the surface plasmon resonance is slightly tunable in visible range by the applied voltage.[76] In the terahertz range, surface plasmon resonances were shown in a 2D gas within a thin InN film manifested through surface electron accumulation efficiently acting as a 2D material.[77]

3.2.2. *Plasmons in ultrathin noble metals*

As plasmonics entered the 2D realm with the advent of graphene plasmonics, there has also been an effort to achieve 2D electron gas (2DEG) with noble metals. Only very recently, El-Fattah et al.[78] demonstrated high-Q (~4) plasmons in the near-infrared range by using lithographically patterned thin silver films. The silver is grown epitaxially allowing the control of the number of layers down to seven Ag(111) layers.

Maniyara et al.[79] have developed a method to evaporate ultrathin gold films of thickness less than 5 nm using copper seeding. Such films are sufficiently thin to exhibit effects similar to those found in 2D metallic materials like graphene. By tailoring the design of Au nanoribbon arrays the plasmonic resonance might be ex-situ tuned from near-infrared to mid-infrared. The plasmonic response of such arrays can be also modulated from 1.9 μm to 2.1 μm in-situ by applying a gate voltage. It has been reported that the nature and quality of the seeding strongly affect the noble metal property and thus the plasmonic performance of the resulting film.[80]

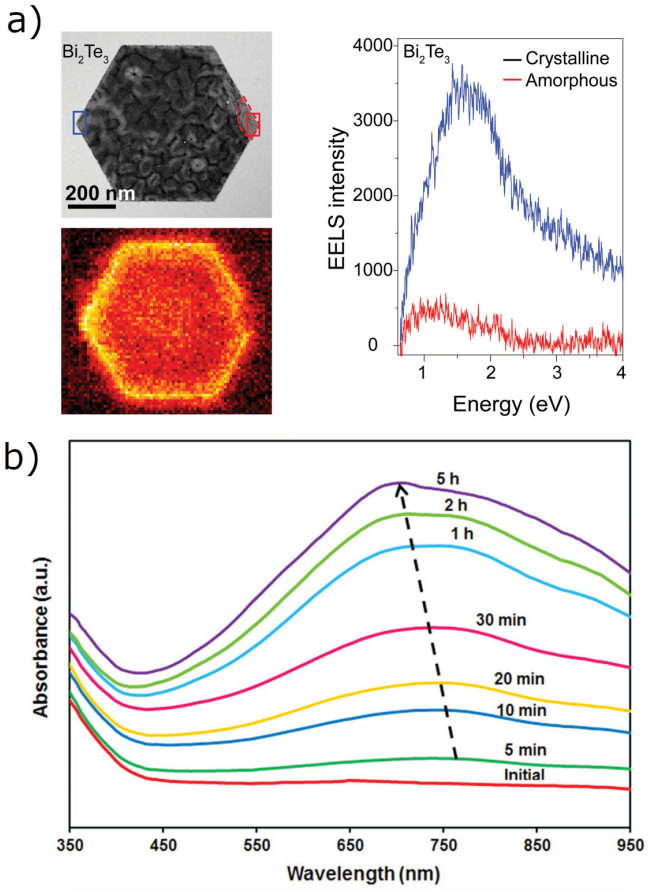

Fig. 3: a) Surface plasmons within Bi_2Te_3 nanoprisms depend on the crystallinity of the material. Reproduced from[71] with permission. Copyright 2016, Wiley-VCH Verlag GmbH & Co. KGaA, Weinheim. b) MoO_3 plasmons can be controlled by irradiation. Reproduced from[74] with permission. Copyright 2014, Wiley-VCH Verlag GmbH & Co. KGaA, Weinheim.

4. The interaction of transition metal dichalcogenides with plasmonic nanostructures

Monolayers of transition metal dichalcogenides (TMDC) have been getting a lot of attention in recent years due to their high exciton binding energies[81], direct bandgap[29], high spin-orbit coupling and no inversion centre implying a valley degree of freedom[82]. TMDC monolayer posses inherently high photoluminescence (PL) yield, which, in the case of MoS_2 and WS_2, can be further improved by defect engineering[83] and chemical treatment up to near-unity values.[84;85]

In combination with plasmonics effects for strong coupling[25], photoluminescence enhancement[86] and spin-valley polarization have been demonstrated[87]. It is noticed that surface plasmons and localized surface plasmons at the interface of metal and TMDC decay through the emission of hot electrons, which are injected into the TMDC to generate a photocurrent.[88;89]

4.1. *Plasmon-exciton polaritons in 2D materials*

Hybridization of surface plasmon modes and excitonic mode leads to the formation of a new quasiparticle called plasmon-exciton polariton. Exciton-polariton, in general, is formed by a coupling between excitons and photons. In the strong coupling regime, coupling larger than the average dissipations may lead to the formation of coherent quantum system and a plethora of interesting effects such as Bose-Einstein condensation[90], enhancing nonradiative energy transfer[91], modifying the chemical reaction rate[92], enhancing conductivity[93], superfluidity, and quantized vortex[25]. Such effects are typically observed at cryogenic temperatures, however large exciton binding energies in TMDC allow some of these effects to be pronounced even at room temperatures.[94] Strong coupling is defined as $g > (\gamma + \kappa)/2$, where γ, κ, and g are damping of the exciton, plasmonic nanocavity and coupling strength of the system respectively. The eigenfrequencies of the field are split, giving rise to new hybrid light-matter states as shown in Figure 4a[25].

On the other hand in the weak coupling regime, the plasmon and exciton modes are unperturbed by the interaction of the surface plasmon electromagnetic field and the exciton dipole in this regime, the absorption cross-section is enhanced and radiation rate is increased, which leads to the effects of surface-enhanced Raman scattering[95] and surface-enhanced fluorescence[96].

4.2. *Strong plasmon-exciton coupling with 2D TMDC semiconductor/metal interface*

Strong plasmon-exciton coupling with 2D TMDC semiconductor/metal interface has been theoretically predicted by Mortensen et al.[99] A Rabi splitting exceeding 100 meV has been calculated with a coupled model for a dielectric/WS_2/gold/WS_2/dielectric structure, while the dielectric has a $\varepsilon_d = 2.1$. Such an interaction has recently been revealed experimentally by introducing Ga nanoparticles as Mie scatterers placed on the Au/WS_2 hybrid structure, which resulted in a clear Rabi splitting in the scattering spectra.[100]

The surface plasmon-exciton interaction has been utilized to create a nonlinear plasmonic modulator. A monolayer WSe_2 encapsulated in hBN is placed onto a plasmonic waveguide, which then shows a pronounced dip in the transmission spectra.[101] Tamm-plasmon-exciton polaritons with a Rabi splitting of 23.5 meV have been observed at room temperature in WSe_2 monolayer embedded inside a structure consisting of SiO_2/TiO_2 distributed Bragg resonator, poly(methyl methacrylate) (PMMA) and a gold layer.[102] Similar architecture with WS_2 achieved a Rabi splitting of 70 meV, however, Fabry-Perot resonance is likely to play a role here rather than Tamm plasmon.[103]

4.3. *Strong coupling of 2D materials with surface lattice resonance*

Plasmonic arrays may exhibit surface lattice resonance manifested by a drastic reduction of the plasmon resonance line-width. The surface lattice resonance means that one of the waves diffracted by the array propagates in the plane of the array.[104] Arrays of plasmonic nanoparticles

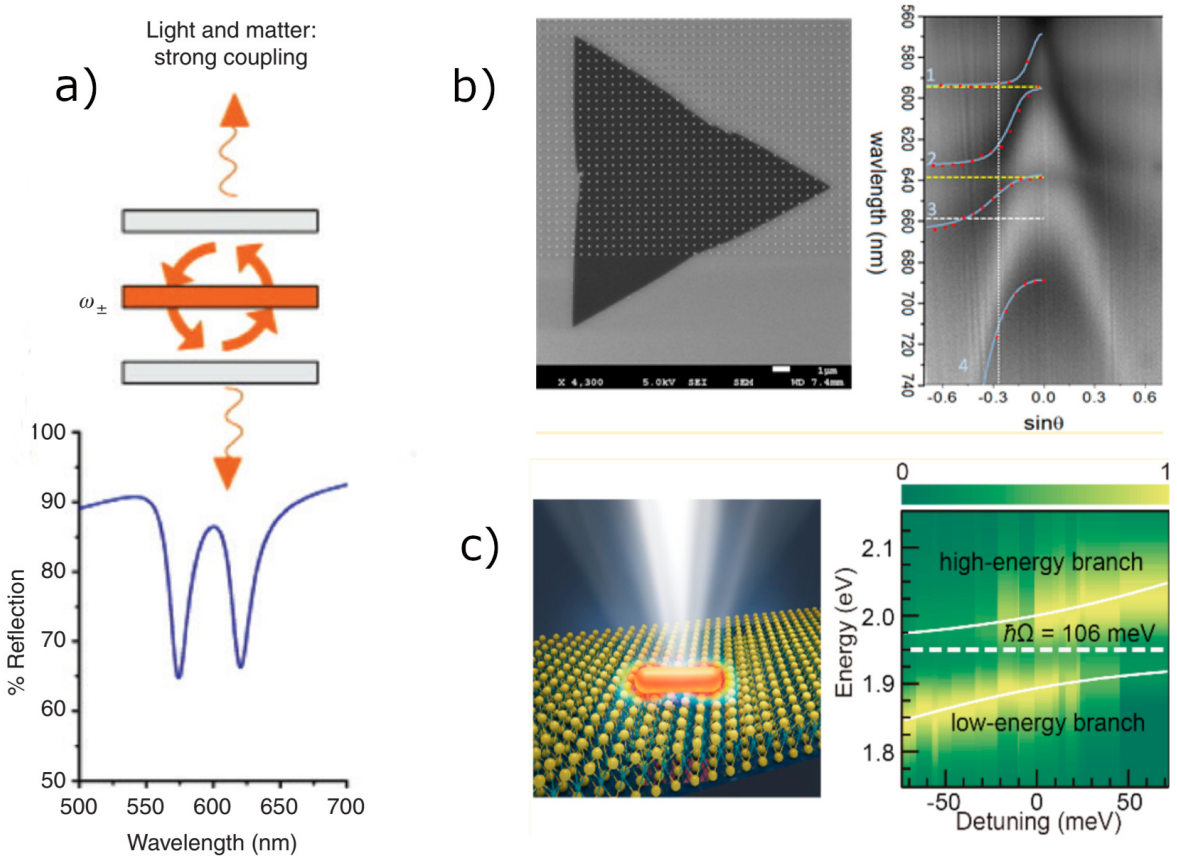

Fig. 4: a) Scheme of the strong coupling principle. The strong coupling is manifested by the Rabi splitting in the extinction spectrum. Reproduced from[97] with permission. Copyright 2018, De Gruyter. b) Coupling of the MoS_2 monolayer to the plasmonic lattice. Reproduced from[98] with permission. Copyright 2016, American Chemical Society. c) Strong coupling of a single gold nanorod with a WS_2 monolayer reaches 106 meV. Reproduced from[47] with permission. Copyright 2017, American Chemical Society

have been widely used for sensing[105], dye-free color printing[106–108], and lasing[109]. Due to their sharp resonances with relatively high quality factors, these arrays are highly beneficial for studies of polaritonic effects[110;111].

Using chemical vapor deposition (CVD) grown MoS_2 monolayer coupled to the array of bowtie nanoantennas, Lee et al.[112] have shown Fano resonances in the reflectance spectrum, which could be controlled by tuning the lattice parameters of the array. In another work, the same group observed a strong coupling of CVD grown MoS_2 monolayer with a plasmonic lattice of silver cylinders with a Rabi splitting of 58 meV at 77 K measured with a Fourier plane imaging setup. (Figure 4b)[98] The effect can be controlled with charge carrier injection and depletion via applying a gate voltage. Not only that the approach allows tuning between weak and strong coupling regimes, but also a new branch of trion resonance emerges at a high doping concentration.[113]

Wang et al.[114] compared a coherent coupling of WS_2 monolayers with Fabry-Perot metallic cavity and plasmonic nanohole array, achieving the Rabi splitting of 101 meV and 60 meV, respectively due to the lower coupling strength of the nanohole array. Stronger coupling was also recently observed with an array of silver nanorods. With an alumina spacer and WS_2 of a different number of layers, Rabi splitting with an energy between 50 meV

for a monolayer and 100 meV for 16 layers of WS_2 were shown.[115] Such a plasmonic lattice was previously used to show plasmon-exciton coupling with organic molecules.[110;111] Very narrow gaps in bowtie nanoantennas have been shown to yield high values of Ω_R up to 138 meV.[116]

4.4. *Strong coupling of 2D materials with a single plasmonic nanoantenna*

A lot of effort has been made to explore the plasmon-exciton interaction between 2D materials and single metallic nanoparticles (NP). Such studies are attractive because they allow studying the strong coupling with low numbers of excitons as the mode volume of plasmonic NPs is very small. Also, high scattering cross-section of these NPs[117] allows this interaction to be studied by using simple optical methods such as dark-field microscopy. Rabi splitting of 135 meV has been observed on nanoparticle on mirror (NPoM) structure with mono- and few-layer WSe_2 stacked between the golden thin film and spherical gold NPs, while detuning had been achieved by irradiating NP with a blue laser to drive Au atoms towards the NP bottom facet, which red-tunes the plasmon.[118] Another way to detune the NPoM nanocavities is by introducing a thin spacer between the metal mirror and the 2D material.[119] Due to their resonance tunability and higher quality factors, plasmonic nanorods offer a convenient platform for studies of strong coupling (Figure 4c).[47] The light-matter interactions can be controlled by encapsulating the plasmonic nanocavity with a thin ALD-grown oxide film red-shifting the resonance peak[120] or by changing the refractive index of the environment with a particular solvent[121]. Mode volume of the nanocavity can be further reduced by employing bipyramids instead of nanorods and exploiting their sharp edges.[122] Even though the Rabi splitting might be anticipated to scale with a square root of the number of layers, in practice, this does not happen because only in-plane coupling contributes to the Rabi energy.[115] While all the aforementioned experiments were performed at room temperature, at a cryogenic temperature more than two polariton branches might arise.[123] Even larger Rabi splitting in the TMDC-plasmonic nanocavity system has been observed for a few-layer WS_2 coupled with gold nanodiscs with a value of 175 meV.[124] However, very recently Hou et al.[125] showed a Rabi splitting of 190 meV with a silver nanocube on a gold mirror nanocavity coupled with CVD grown MoS_2 monolayer.

In the intermediate coupling regime, both an anti-crossing dispersion curve and photoluminescence enhancement are observed. Using a nanoparticle on mirror geometry with silver film, alumina spacer, polyvinylpyrrolidone (PVP) coated silver nanocubes, Sun et al.[126] managed to observe a Rabi splitting of 36.7 meV and a local photoluminescence enhancement with a factor of 1700x in WSe_2. In that case, the Purcell effect still applies and photoluminescence is enhanced by plexcitons.

4.5. *Tunability of the strong-coupling interaction*

One of the big advantages of using semiconducting 2D monolayers is their tunability. By applying the gate voltage, the refractive index in the exciton resonances region changes. In the case of WS_2, the change can be as high as 60% for the imaginary part and 20% for the real part of the complex refractive index. The effect is attributed to the spectral width broadening of the excitonic interband transitions.[127] Slight tunability using a gold layer as a back gate and Si_3N_4 as a gate dielectric has been also shown for MoS_2 and applied for light modulators achieving 10% tunability.[128] The tunability can be also applied to control the strong coupling of TMDC in a cavity. By embedding a WS_2 monolayer in a cavity formed by two silver mirrors, a thin Al_2O_3 layer and a PMMA layer, complete control of the strong coupling has been shown when a gate voltage was applied.[129]

Exploiting this property allows fabrication of tunable hybrid 2D-plasmonic devices.[113;130] By embedding an MoS_2 monolayer in a structure comprised by a gold mirror working as a back gate, SiO_2 spacer and a gold nanostrip array, Ni et al.[131] were able to electrically control the emission of exciton-plasmon polaritons.

4.6. *Plasmon enhanced absorption and photoluminescence in 2D materials*

Based on different plasmonic structures, the PL in semiconducting 2D materials could be enhanced[132–137]. The main mechanism of PL enhancement is to increase the absorption (excitation field at the pump wavelength) and scattering emission (at the PL emission wavelength) through enhancing light-matter interactions of the active materials in the vicinity of the plasmonic nanostructures[132;133;136–138]. The absorption enhancement could be achieved in low dimensional materials by hybridizing them with different structures of plasmonic materials, while the enhanced emission relies on the Purcell effect[86;139], which enhances the rate of spontaneous emission when a dipole emitter is placed inside a cavity resonator. The enhancement factor (FP) due to the Purcell effect is defined by this formula[139].

$$\mathsf{FP} = (\frac{3}{4}\pi^2)(\frac{\lambda_0}{\mathfrak{n}})^3(\frac{\mathsf{Q}}{\mathsf{V_m}}), \tag{8}$$

where λ_0, $\mathfrak{n}$, Q, and $\mathsf{V_m}$ denote the emitter's free space wavelength (resonance wavelength of the plasmonic materials), the refractive index of the cavity (for example plasmonic substrate), the quality factor of the cavity and its mode volume, respectively. One can see from this formula that the higher FP could be achieved either by increasing the quality factor or decreasing its mode volume.

A lot of research has been conducted for enhancing the plasmonic properties of 2D materials. Wang et al.[86] observed 20000-fold of the PL enhancement factor in WSe_2 transferred on a gold substrate patterned with trenches of lower than 20 nm wide (Figure 5a, b). They used different pump wavelengths as well as different pitch sizes for optimizing the maximum resonance and the corresponding PL enhancement factor. They reported the best PL enhancement of WSe_2/Au due to enhanced absorption and FP could be achieved by using a 633 nm pump laser with a pitch size of 200 nm and sub-20 nm-wide trenches. With silver nanoparticles fabricated by annealing a thin Ag film, Zhao et al.[140] showed enhancement with a factor of 30 for MoS_2. On the other hand, WS_2 with a much higher intrinsic quantum yield got PL quenched and only got slightly enhanced when using an hBN spacer. Moreover, they had shown induced transparency in $MoSe_2$ which is a signature of an efficient plasmon-exciton coupling.

Single crystalline gold nanorods have also been used to demonstrate plasmon-enhanced photoluminescence within TMDC. With these, Kern et al.[141] showed an one order of magnitude of PL enhancement within WS_2 attributed to a combined effect of absorption (Figure 5c) and emission enhancement. It has been shown that the PL enhancement factor of MoS_2 increases with the coverage of gold nanorods until the density of around 40 μm^{-2} and then decreases again (Figure 5d). That is attributed to the prevailing absorption of the nanorods.[142]

Butun et al.[132] employed a plasmonic structure of silver discs with different diameters on the top of pristine MoS_2 and they noticed an overall enhancement of PL by 12-fold with the disc diameter of 130 nm. Later, the same group used sapphire substrate to quantify the enhanced light absorption in WS_2 using different disc diameters (90, 100 and 115 nm) and showed a four-fold increase in the absorption of Ag discs array/WS_2 at the disc diameter of 100 nm as shown at Figure 5e.[133]

4.7. *Surface enhanced Raman scattering*

Surface-enhanced Raman scattering is a well-known phenomenon, commonly used for ultrasensitive sensing.[95] It is based on the fact, that the cross-section of the Raman scattering is proportional to the local intensity of the electric field resulting in a dramatic enhancement of Raman scattering.[51] Recently, a new fully quantum description of the enhancement as a nanocavity coupled to the emitter has attracted a lot of attention[143;144]. The 2D nature of TMDC allows studies of the Raman enhancement and related quantum phenomena in subnanometer gaps. Using nanoparticle on mirror geometry Chen et al.[145] confirmed previous reports describing a low limit for the gap size below which the Raman enhancement decreases rather than increases. This limit is given by a quantum tunneling effect.[146] Enhancement of Raman scattering within TMDC has also been shown using gold nanoparticles[147] and Tip-Enhanced Raman Scattering (TERS), where a

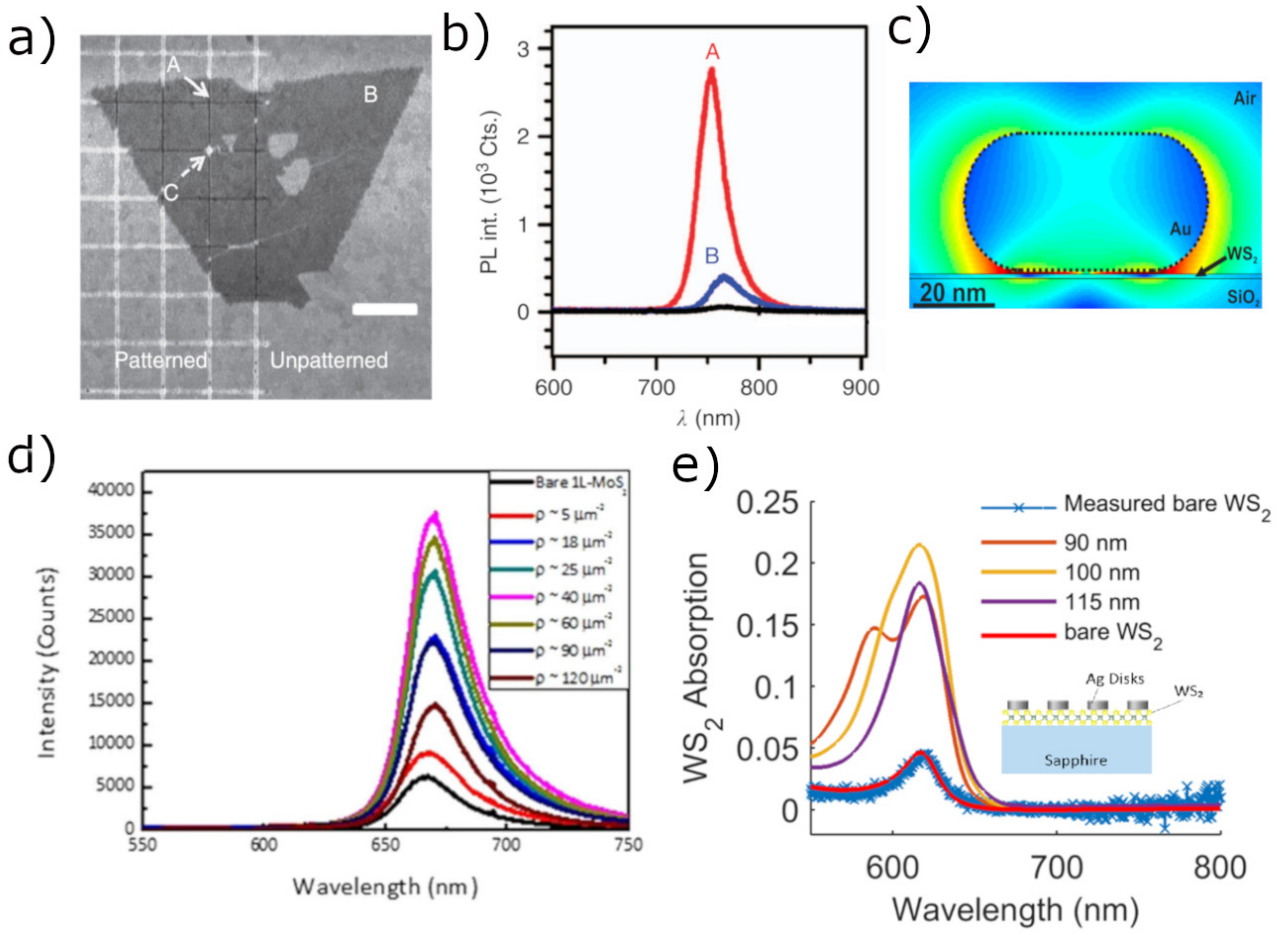

Fig. 5: The photoluminescence of WSe_2 monolayer on patterned gold substrate a) is strongly enhanced in the narrow hot-spots b). Reproduced from[86] with permission. Copyright 2016, Macmillan Publishers Ltd. c) The finite difference time domain simulation of the gold nanorod on the top of WS_2 monolayer shows the confinement of the electromagnetic field to the monolayer. Reproduced from[141] with permission. Copyright 2015, Amerian Chemical Society. d) The coverage of the gold nanorods influence the enhancement of photoluminescence. Reproduced from[142] with permission. Copyright 2015, Macmillan Publishers Ltd. e) Ag nanodiscs on MoS_2 dramatically increase absorption. Reproduced from[133] with permission. Copyright 2017, American Chemical Society.

metalized tip is used to scan the Raman image of the sample.[148]

A hybrid van der Waals heterostructures of MoS_2 or WS_2 nanodomes and graphene were found to be an excellent SERS subtrate with a capability to detect Rhodamine 6G (R6G) molecules in concentrations as low as $5x10^{-12}$ M.[149] MoS_2/graphene heterostructure also provides SERS enhancement when combined with gold nanoparticles. Such a heterostructure leads to a SERS sensitivity one order higher than without any MoS_2. R6G in a concentration of $5x10^{-10}$ was detected when using 532 nm laser in resonance with the nanoparticles.[150] MoS_2 nanosheets chemically exfoliated using NaK metal alloy also provide a possible platform for SERS detection. The hybrid NaK-MoS_2 plasmonic-2D structure allows the detection of R6G down to the concentration of $10^{-}9$ M.[151]

4.8. *Valley polarization*

Due to the absence of the inversion symmetry, strong spin-orbit coupling and a direct bandgap at both K and K' valleys lead to two classes of excitons addressable by different polarization of light.[82] Interest in these effects has led to the creation of a new field of valleytronics with potential applications in quantum computing.[152]

As demonstrated using Tamm-plasmon structure, tailored electrodynamic environment leads to an enhancement of the valley polarization.[153] Gong et al.[87] demonstrated the valley-directional coupling of a silver nanowire with five layers of WS_2. Using a plasmonic metamaterial consisting of an array of asymmetric grooves Sun et al.[154] were able to spatially separate valley polarized excitons in a MoS_2 monolayer. $\sigma+$ polarized light excites excitons in K valley, while $\sigma-$ excites excitons in K' valley and these excitons coupled to the guided surface plasmon polaritons propagate in the opposite directions. With a metal film-over-nanosphere plasmonic-photonic crystal coupled with WS_2 monolayer, Ding et al.[155] managed to observe a room temperature Rabi splitting of 160 meV in transmission spectra and valley polarized photoluminescence tunable by the excitation angle.

A combination of an optical spin-orbit mode with TMDC monolayers yields a spin-selective excitation of polaritons with a 5-8% coherence and 40% intervalley contrast.[156] The valley coherence might be improved by a second harmonic generation process within a chiral plasmonic metasurface coupled with a WS_2 monolayer which allows a steering of valley-polarized photons at a room temperature. The field confinement provided by the plasmonic metasurface leads to an enhancement of the second harmonic generation. Due to the valley locking the photons can be steered without external stimuli like an electric or magnetic field.[157]

Atomic force microscope allows a manipulation of gold nanorods to create a sandwich Au NR/MoS_2/Au NR structure. Such a design leads to a modulation of valley-polarized photoluminescence reaching the degree of valley polarization of 47% compared to 18% in the case of a bare MoS_2. In addition the photoluminescence is enhanced by three orders of magnitude.[158]

4.9. *Plasmonic control of dark exciton emission*

The electron-hole charge exchange and conduction band spin-splitting imply a splitting between bright and dark excitonic states.[159] These dark excitons involve spin-forbidden transition and cannot be normally accessed by far-field optical techniques but their emission has been observed using a plasmonic structure.

By near-field coupling of WSe_2 monolayer to a surface plasmon polariton in a single crystalline silver film, Zhou et al.[160] managed to probe the dark excitons at the temperature of 4K. Such a method offers a convenient way to probe near-field effects without the necessity for near-field microscopes. More recently, Park et al.[161] used tip-enhanced photoluminescence to control the dark emission within WSe_2 monolayer on a gold substrate at room temperature. In this experiment, metal-coated tip is used as a probe employing the Purcell effect.

Dark excitons modify the linewidth of the Fano resonance in the hybrid structure of WS_2 and stacked gold nanotriangles. The out-of-plane dipole moment of the stacked nanotriangles leads to the coupling with the dark K-K excitons and reduces the A exciton spectral linewidth.[162]

5. Applications

5.1. *Photodetectors*

A photodetector (PD), which is a device that absorbs photons and converts them into electrical signals, is used in many fields including optical communications, environmental monitoring, military, and security.[163] High-performance 2D PDs based on plasmonic materials can achieve a subdiffraction-limited light confinement and enhance the resonant electric field.[138] The detection in 2D plasmonic PDs (PPDs) could be categorized into two main mechanisms. The first one is to increase the absorption and create more electron-hole (e-h) pairs in the 2D semiconductor materials used for photodetection by making use of the localized surface plasmon resonance (LSPR) of the plasmonic material (Figure 6a). In this case, the plasmonic materials are used as optical antennas to confine the light (with energy larger than bandgap energy) in 2D semiconductor at the resonant wavelength of the plasmonic material. In the second

mechanism, Schottky junction is formed between the metal nanoparticle and the semiconductor surface. Thus, the internal photoemission of the hot carriers could be improved by the enhanced absorption at the metal nanoparticle.[164]

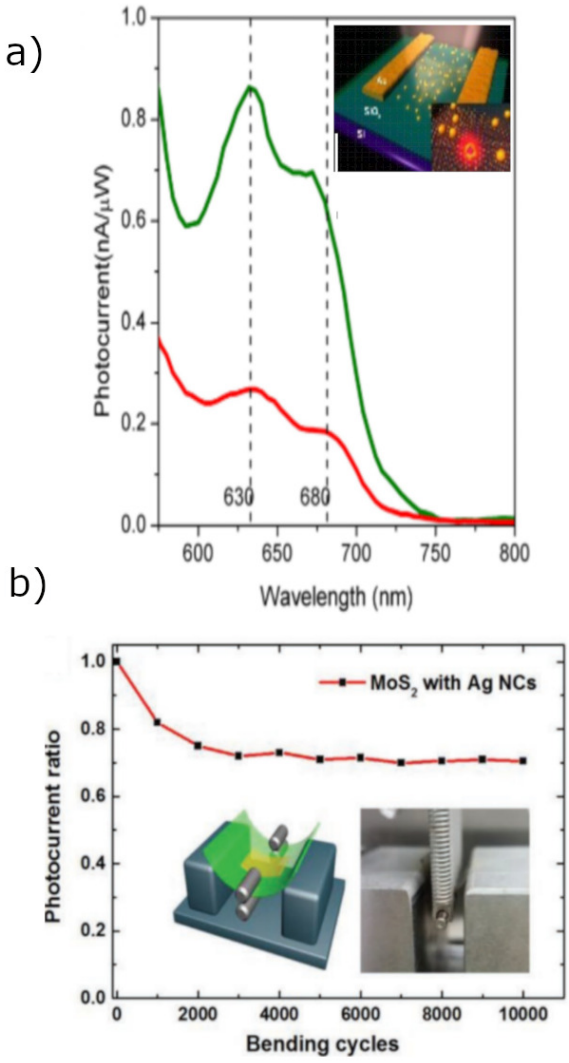

Fig. 6: a) Photocurrent and scheme of MoS_2 monolayer with (green) and without (red) Au nanoshells on the MoS_2. Reproduced from[135] with permission. Copyright 2014, AIP Publishing. b) Scheme, photograph and normalized photocurrent of the flexible photodetector as a function of bending cycles. Reproduced from[165] with permission. Copyright 2017, Wiley-VCH Verlag GmbH & Co. KGaA, Weinheim.

Many approaches have been proposed to demonstrate a high-performance 2D-PPDs such as depositing metal NPs. The LSPR could be tuned to match the band of the PD by controlling the diameter of the deposited NPs which increases the absorption of the trapped electric field on the NPs surface absorption and the detectivity of the PD.[138] Liu et al.,[166] demonstrated a phototransistor based on hybridizing the graphene with Au nanoparticles by annealing the Au thin films deposited on silica substrates and transfering the remaining Au nanoparticles to the graphene phototransistor. Depending on the Au film thickness, Au nanoparticles exhibited the enhancement of the LSPR and photocurrent in the wavelength range from 500 to 700 nm. They reported 10 to 15-fold enhancement in photocurrent with a responsivity of 6.1 mA/W using 110 nm diameter of Au nanoparticles (corresponding to 12 nm film thickness). Other graphene-based PPDs were demonstrated, for example, 8-fold enhancement of the photocurrent by using arrays of Au heptamer antennas sandwiched between 2 graphene layers.[167] Through this configuration, the authors achieved 20% internal quantum efficiency and a maximum responsivity of 13 mA/W.

Together with graphene, other 2D-PPDs based on TMDC have been demonstrated. Using chemical doping on a few layer WS_2 with a thickness of 3 nm by Ag nanoparticles (4-6 nm size) coated with polyvinylpyrrolidone (PVP), Chowdhury et al.[168] fabricated an n-WS_2/p-Si PD with a maximum photoresponsivity and detectivity of 8 A/W and $1.5x10^{10}$ Jones, respectively. This design enables exploiting the entanglement of the plasmonic absorption peak of Ag (~420 nm) and the band-edge absorptions of WS_2 (~525 and 630 nm). They reported also an enhancement of the external quantum efficiency (EQE) of ~2000 %. Mukherjee et al.[136] reported a 5-times increase in the average absorption of MoS_2 monolayer over a broadband spectral range from 400 to 800 nm using Au NPs.

MoS_2 is the most studied TMDC material as a PPD, and field-effect-transistors (FETs) based on MoS_2 have been demonstrated by several groups.[134;135;137] Using silica-gold nanoshell structures, Sobhani et al.[135] demonstrated FET based on MoS_2 monolayer (Figure 6a) with a threefold increase in the photocurrent and double increase of the PL signal due to the enhanced absorption in the MoS_2 at the resonant wavelength. Figure 6b shows the photocurrent of the device.

They used plasmonic silica-gold nanoshells with 60 nm SiO_2 core size and 30 nm Au shell. Another group integrated silica-gold nanoshells of the same size of Au shell (30 nm) but different designs and a different silica core size of 83 nm with a MoS_2 monolayer and they observed larger PL emission enhancement about 10-fold.[134] Bang and co-workers[169] demonstrated a high-performance MoS_2 PPD using a network of Ag nanowires encapsulated with the PVP layer. The PVP layer here is used as a trap site for capturing the charges, resulting in 250x increase in the photocurrent of the hybrid structure as compared with the pristine MoS_2 monolayer.

With 110-fold PL enhancement and responsivity of 287.5 A/W, Wu et al.[170] constructed a gap-mode PPD based on Ag nanoshell/MoS_2/Au NPoM structure. This enhancement was achieved by using an insulating layer of Al_2O_3 to prevent the charge transfer between metal NPs and MoS_2. Sun et al.[171] used a similar NPoM architecture employing silica coated Ag nanocubes, MoS_2, SiO_2 as an insulating layer, and Ag thin layer on a flexible substrate. Such a device yields a 139-fold PL enhancement and 38-fold enhanced photoresponsivity (7940 A/W). More interestingly, using this design, the authors noticed only a reduction to 71 % in the photocurrent ratio of the device after bending for 10000-times, which indicates the good mechanical properties of the device. Apart from Au and Ag plasmonic nanostructures, other materials were also used for PPD, for example, Pt nanostripes.[165] Different from Au and Ag, Pt shows broad LSPR ranging from UV to near IR enabling a broadband PPD Pt nanostrip/bilayer MoS_2. They reported photoresponsivites of 14, 312.5 and 69.2 A/W in the UV, visible and near IR range respectively.

5.2. *Surface plasmon biosensors*

Sensing is one of the primary applications of plasmonic nanostructures.[172–174] The interaction between 2D materials and surface plasmon polaritons can be exploited to increase the sensitivity of surface plasmon resonance (SPR) biosensors. In these sensors, a surface plasmon is excited on the interface between a metal film and a dielectric superstrate, which is typically functionalized with biorecognition elements. As the refractive index of the superstrate changes with the adsorption of the analyte, the change of the plasmon propagation constant yields a change in the plasmon wavelength or the resonant angle, phase and polarization of the optical wave, which can be measured.[50] Figure 7a shows the basic configurations of SPR sensors exciting surface plasmon polariton using a prism, grating or a waveguide.[1]

Due to their atomic layer thicknesses, 2D materials are highly beneficial for the improvement of SPR sensors sensitivity since they allow the fine tuning of the refractive index with atomic precision. Graphene biosensors based on surface plasmon resonance was proposed in 2010 by Wu et al.[175] Graphene, in this case, has two functions. It adsorbs biomolecules and thus can be used as a molecular recognition element. Moreover, the high refractive index of graphene modifies the optical response of the sensor by enhancing the absorption and increases the sensitivity.

Several other sensor architectures utilizing 2D materials including both graphene[176] and other materials have been theoretically proposed in recent years. Ouyang et al.[177] proposed a sensor utilizing 7 nm Si film and a WS_2 monolayer reaching theoretical sensitivity of 155 deg/RIU. Same approach can be employed for phase-sensitive detection with a phase sensitivity of $1.1\text{x}10^7$ deg/RIU compared to that of $1.2\text{x}10^4$ deg/RIU for conventional phase-sensitive SPR sensor.[178] Other proposed architectures includes utilising few-layer black phosphorus[179], Tin Selenide allotropes[180] or MoS_2/Aluminium/MoS_2/graphene structure.[181] An ultrahigh sensitivity of 540.8 deg/RIU has been designed with a graphene/MoS_2 heterostructure, KCl absentee layer and a low-refractive index MgF_2 prism.[182]

Other designs focused on long-range plasmons, where the surface plasmon polaritons are guided using a hybrid plasmonic-waveguide structure.[183] Xu et al.[184] proposed a design in which the surface plasmons are guided with a 300 nm of a CYTOP^{TM} and Au is only 20 nm thick. 6 layers of MoS_2 are located between gold and the analyte achieving twice the imaging sensitivity and 10 times the detection accuracy compared to a bare 50 nm of gold. Wu et al.[185] showed a maximum sensitivity

enhancement of 98% for a guided wave sensor with silicon and MoS_2/graphene heterostructure with six layers of MoS_2.

Wang et al.[186] saw a 26% increase of sensitivity when coating the SPR sensor with WS_2 nanosheets. However, it is necessary to point out, that in this case, WS_2 was not in the form of a 2D film but a rather non-uniform coating with a thickness of several hundred nm. Due to the difficulties in the growth of a large area TMDC, these sensors are still mostly theoretical concepts. However, some efforts have been made on the experimental side.

Chiu et al.[187] developed a graphene/Au SPR chip capable of detection of BSA in concentrations as low as 100 pg/ml which is a 100 fold improvement compared to a conventional sensor. Furthermore, at a higher concentration of 75 nM, the angle shift was 1.4x higher than in the case of a conventional SPR sensor.

5.3. *Metasurfaces*

Metasurfaces are the two-dimensional equivalent of metamaterials, composing discrete subwavelength structures, possessing the capability of full control of light properties such as amplitude, phase, dispersion, momentum, and polarization[188]. Due to their unique ability to manipulate electromagnetic waves from microwave to UV spectra, metasurfaces for various applications, such as frequency-selective metasurfaces[108;189–191], high-impedance metasurfaces[192;193], perfectly absorbing metasurfaces[194–196], and wave-front shaping metasurfaces[197–203] have been demonstrated. Moreover, metasurfaces provide ultra-thin feature and easiness for integration compared with conventional refractive optics. Active control of light propagation has gained practical and fundamental significance[204]. For example, tunable frequency selective or perfectly absorbing metasurfaces allow accurate resonance tuning to perfectly match the operational condition or switching of operational frequency in signal modulation[205–207]. Another example is tunable beam steering which has many applications such as LIDAR and holography display[208;209] or it could be used in designing a lens with tunable focal length[210;211].

Two-dimensional (2D) materials have attracted tremendous attention in the design of tunable metasurfaces due to their unprecedented properties, specifically tunable Fermi level, which is done using a small bias gate voltage[23;212]. They also possess high carrier mobility which makes them a desirable candidate as a plasmonic material with low loss[213].

Some of the tunable metasurfaces comprise metal or dielectric resonators with a monolayer of tunable graphene[213–218]. On the other hand, patterned graphene is also used as the resonator in a unit cell of tunable metasurfaces[63;219–221]. Multilayers of graphene and dielectric or ferroelectric materials are also used to tune different properties of the metasurfaces[222;223]. Other 2D materials such as molybdenum disulfide (MoS_2) are also used in designing tunable absorber metasurfaces. Ni et al.[131] designed a tunable light-emitting plasmonic metasurface based on an array of gold nanowires and Petoukhoff et al.[224] demonstrated an enhanced charge transfer and absorption hybrid MoS_2-organic heterojunction using a plasmonic metasurface.

6. Summary and outlook

In this review, we showed recent progress in 2D plasmonics. Novel materials for the realization of plasmonic structures in two dimension are emerging. Furthermore the research on the interactions between semiconducting 2D materials and plasmonic nanostructures have been very fruitful. We reviewed emerging applications based on 2D plasmonics such as surface plasmon biosensors, photodetectors, and metasurfaces.

It is reasonable to expect that 2D tunable plasmonic metamaterials will emerge into a new interesting field. Especially low-loss 2D plasmons in visible and NIR range excitable from a free space are highly desirable for a range of applications.

Strong exciton-plasmon coupling observable at room temperatures and completely tunable by an electric gating might find applications in quantum information processing as cavity quantum electrodynamics have been proposed as a good platform for quantum computing.[225]

Polaritonic LED was recently shown using a distributed Bragg reflector microcavity[226] but

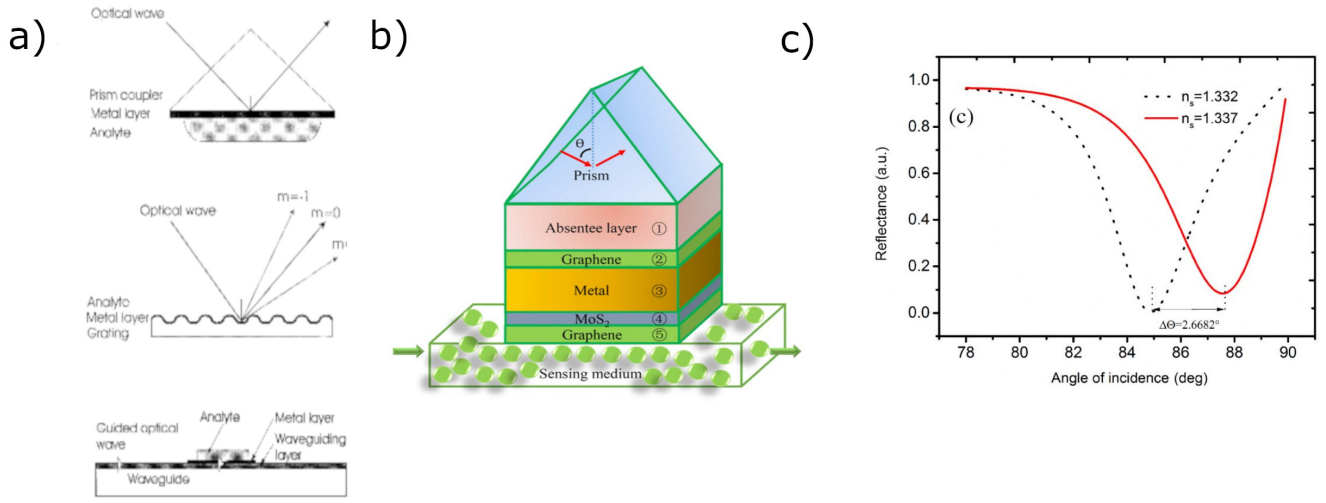

Fig. 7: a) Configurations of SPR sensors - prism coupling, grating coupling and integration with a waveguide. Reproduced from [1] with permission. Copyright 1999, Elsevier. b) Proposed design c) and surface plasmon resonance shift of ultrasensitive SPR sensor based on graphene and MoS_2. Reproduced from [182] with permission. Copyright 2018, Optical Society of America.

such a device might as well be constructed using a plasmonic cavity. So far, a light-emitting diode exploits a fluorescence resonance energy transfer (FRET) from silver nanoparticles to TMDC monolayer, resulting in focused electroluminescence with a narrow excitonic resonance.[227] Furthermore, MoS_2 and WS_2 chemically treated with bis(trifluoromethane) sulfonimide have exhibited near-unity photoluminescence[84] and increased electroluminescence.[37] Combining these with plasmonic structure might bring exciting applications.

Plasmonic lasers using traditional semiconducting materials have been around for approximately 10 years.[109;228] Plasmonic lasing using 2D materials would be an interesting development to observe in the near future. The use of TMDC potentially offer tunable lasing, variability using heterostructures[229;230] and improved applications in laser-enhanced sensing,[231] and low thresholds.

It is reasonable to expect that ultrasensitive surface plasmon resonance biosensors will be experimentally demonstrated following a variety of theoretical proposals.

So far, the tunable properties of the 2D materials are explored extensively with combination with plasmonic resonators to design variety of tunable metasurfaces. Although the results of some these metasurfaces look promising, challenge remains in the fabrication of large-area 2D materials. In order to integrate these metasurfaces in the real user-end devices, a repeatable and realible fabrication of 2D materials for large scale production is required.

Acknowledgments

MS thanks UCL and the ARAP program of A*STAR for the scholarship and facilities. The work is supported by the Agency for Science, Technology and Research (A*STAR) under 2D Materials Pharos Program (Grant No. 152 700014) and IAF-PP TBIP@SBIC (Grant No. H19H6a0025).

References

1. J. Homola, *et al.*, *Sensors and Actuators B: Chemical* **54**, 3 (1999).
2. B. Liedberg, *et al.*, *Sensors and actuators* **4**, 299 (1983).
3. G. Qiu, *et al.*, *ACS nano* p. DOI: 10.1021/acsnano.0c02439 (2020).
4. S. A. Maier, *Plasmonics: fundamentals and applications* (Springer Science & Business Media, 2007).
5. N. T. K. Thanh, Z. Rosenzweig, *Analytical Chemistry* **74**, 1624 (2002).
6. R. M. Pallares, *et al.*, *Chemical Communications* **51**, 14524 (2015).
7. R. M. Pallares, *et al.*, *Chemical Communications* **54**, 11260 (2018).
8. X. Huang, *et al.*, *Journal of the American Chemical Society* **128**, 2115 (2006).
9. H. Wang, *et al.*, *Proceedings of the National Academy of Sciences* **102**, 15752 (2005).
10. N. J. Durr, *et al.*, *Nano Letters* **7**, 941 (2007).
11. A. M. Alkilany, *et al.*, *Advanced Drug Delivery Reviews* **64**, 190 (2012).
12. F. Demir Duman, *et al.*, *Journal of Materials Chemistry B* p. DOI: 10.1039/D0TB00810A (2020).
13. T. Niidome, *et al.*, *Journal of Controlled Release* **114**, 343 (2006).
14. N. T. Thanh, L. A. Green, *Nano Today* **5**, 213 (2010).
15. A. Boltasseva, H. A. Atwater, *Science* **331**, 290 (2011).
16. F. Garcia-Vidal, *et al.*, *Journal of Optics A: Pure and Applied Pptics* **7**, S97 (2005).
17. R.-M. Ma, R. F. Oulton, *Nature Nanotechnology* **14**, 12 (2019).
18. A. Kristensen, *et al.*, *Nature Reviews Materials* **2**, 1 (2016).
19. M. S. Schmidt, *et al.*, *Advanced Materials* **24**, OP11 (2012).
20. H. Liu, J. Teng, *Journal of Molecular and Engineering Materials* **1**, 1250005 (2013).
21. L. Pan, *et al.*, *Scientific Reports* **1**, 175 (2011).
22. F. Keilmann, R. Hillenbrand, *Philosophical Transactions of the Royal Society of London. Series A: Mathematical, Physical and Engineering Sciences* **362**, 787 (2004).
23. K. S. Novoselov, *et al.*, *Nature* **438**, 197 (2005).
24. L. Britnell, *et al.*, *Science* **340**, 1311 (2013).
25. C. Schneider, *et al.*, *Nature Communications* **9**, 2695 (2018).
26. E. Hwang, *et al.*, *Physical Review Letters* **98**, 186806 (2007).
27. A. Gupta, *et al.*, *Progress in Materials Science* **73**, 44 (2015).
28. A. K. Geim, I. V. Grigorieva, *Nature* **499**, 419 (2013).
29. K. F. Mak, *et al.*, *Physical Review Letters* **105**, 136805 (2010).
30. P. Rivera, *et al.*, *Nature Communications* **6**, 1 (2015).
31. A. Ciarrocchi, *et al.*, *Nature Photonics* **13**, 131 (2019).
32. D. Unuchek, *et al.*, *Nature* **560**, 340 (2018).
33. M. Zhao, *et al.*, *ACS Applied Materials & Interfaces* **10**, 44102 (2018).
34. T. Roy, *et al.*, *ACS Nano* **8**, 6259 (2014).
35. Q. H. Wang, *et al.*, *Nature Nanotechnology* **7**, 699 (2012).
36. F. Withers, *et al.*, *Nature Materials* **14**, 301 (2015).
37. D.-H. Lien, *et al.*, *Nature Communications* **9**, 1 (2018).
38. Y. Ye, *et al.*, *Nature Photonics* **9**, 733 (2015).
39. S. Wu, *et al.*, *Nature* **520**, 69 (2015).
40. J. Cheng, *et al.*, *Advanced Optical Materials* **7**, 1800441 (2019).
41. S. Lukman, *et al.*, *Nature Nanotechnology* pp. 1–8 (2020).
42. L. Wang, *et al.*, *Small Methods* **2**, 1700294 (2018).
43. T. W. Ebbesen, *et al.*, *Physics Today* **61**, 44 (2008).
44. Y. Li, *et al.*, *Advanced Science* **4**, 1600430 (2017).
45. F. J. Garcia de Abajo, *ACS Photonics* **1**, 135 (2014).
46. A. Woessner, *et al.*, *Nature Materials* **14**, 421 (2015).
47. J. Wen, *et al.*, *Nano Letters* **17**, 4689 (2017).
48. H. Raether, *Surface plasmons on smooth and rough surfaces and on gratings* (Springer-Verlag Berlin An, 2013).

49. J. Wang, *et al.*, *Sensors* **17**, 2719 (2017).
50. J. Homola, *Chemical Reviews* **108**, 462 (2008).
51. P. L. Stiles, *et al.*, *Annual Review of Physical Chemistry* **1**, 601 (2008).
52. C. F. Bohren, D. R. Huffman, *Absorption and scattering of light by small particles* (John Wiley & Sons, 2008).
53. P. G. Etchegoin, *et al.*, *The Journal of Chemical Physics* **125**, 164705 (2006).
54. K. A. Willets, R. P. Van Duyne, *Annual Review of Physical Chemistry* **58**, 267 (2007).
55. A. Grigorenko, *et al.*, *Nature Photonics* **6**, 749 (2012).
56. F. H. Koppens, *et al.*, *Nano Letters* **11**, 3370 (2011).
57. A. C. Neto, *et al.*, *Reviews of Modern Physics* **81**, 109 (2009).
58. Z. Fei, *et al.*, *Nano letters* **11**, 4701 (2011).
59. H. Hou, *et al.*, *Optics Communications* **370**, 226 (2016).
60. D. Rodrigo, *et al.*, *Science* **349**, 165 (2015).
61. J. Chen, *et al.*, *Nature* **487**, 77 (2012).
62. Z. Fei, *et al.*, *Nature* **487**, 82 (2012).
63. L. Ju, *et al.*, *Nature Nanotechnology* **6**, 630 (2011).
64. Y. Li, *et al.*, *Nano Letters* **14**, 1573 (2014).
65. I. A. Calafell, *et al.*, *npj Quantum Information* **5**, 37 (2019).
66. B. Wang, *et al.*, *Applied Physics Letters* **100**, 131111 (2012).
67. B. Wang, *et al.*, *Physical Review Letters* **109**, 073901 (2012).
68. P. R. West, *et al.*, *Laser & Photonics Reviews* **4**, 795 (2010).
69. T. M. Mattox, *et al.*, *Advanced Materials* **27**, 5830 (2015).
70. M. Zhao, *et al.*, *Nano Letters* **15**, 8331 (2015).
71. M. Zhao, *et al.*, *Advanced Materials* **28**, 3138 (2016).
72. Y. Lu, *et al.*, *Journal of the Optical Society of America B* **33**, 1842 (2016).
73. S. D. Lounis, *et al.*, *The Journal of Physical Chemistry Letters* **5**, 1564 (2014).
74. M. M. Alsaif, *et al.*, *Advanced Materials* **26**, 3931 (2014).
75. H. Cheng, *et al.*, *Advanced Materials* **27**, 4616 (2015).
76. Y. Wang, *et al.*, *Nano Letters* **15**, 883 (2015).
77. K. K. Madapu, *et al.*, *Nanotechnology* **29**, 275707 (2018).
78. Z. E.-F. Abd, *et al.*, *ACS Nano* **13**, 7771 (2019).
79. R. A. Maniyara, *et al.*, *Nature Photonics* **13**, 328 (2019).
80. H. Liu, *et al.*, *ACS Nano* **4**, 3139 (2010).
81. B. Zhu, *et al.*, *Scientific Reports* **5**, 9218 (2015).
82. K. F. Mak, *et al.*, *Nature Nanotechnology* **7**, 494 (2012).
83. H. Nan, *et al.*, *ACS Nano* **8**, 5738 (2014).
84. M. Amani, *et al.*, *Science* **350**, 1065 (2015).
85. H. Kim, *et al.*, *ACS Nano* **11**, 5179 (2017).
86. Z. Wang, *et al.*, *Nature Communications* **7**, 11283 (2016).
87. S.-H. Gong, *et al.*, *Science* **359**, 443 (2018).
88. T. Hong, *et al.*, *ACS Nano* **9**, 5357 (2015).
89. M. L. Brongersma, *et al.*, *Nature Nanotechnology* **10**, 25 (2015).
90. R. Balili, *et al.*, *Science* **316**, 1007 (2007).
91. D. Dovzhenko, *et al.*, *Nanoscale* **10**, 3589 (2018).
92. A. Thomas, *et al.*, *Angewandte Chemie International Edition* **55**, 11462 (2016).
93. E. Orgiu, *et al.*, *Nature Materials* **14**, 1123 (2015).
94. L. Zhang, *et al.*, *Nature Communications* **9**, 713 (2018).
95. K. Kneipp, *et al.*, *Physical Review Letters* **78**, 1667 (1997).
96. E. Fort, S. Grésillon, *Journal of Physics D: Applied Physics* **41**, 013001 (2007).
97. E. Cao, *et al.*, *Nanophotonics* **7**, 145 (2018).
98. W. Liu, *et al.*, *Nano Letters* **16**, 1262 (2016).

99. P. Gonçalves, *et al.*, *Physical Review B* **97**, 041402 (2018).
100. F. Deng, *et al.*, *Laser & Photonics Reviews* **14**, 1900420 (2020).
101. M. Klein, *et al.*, *Nature Communications* **10**, 1 (2019).
102. N. Lundt, *et al.*, *Nature Communications* **7**, 13328 (2016).
103. L. C. Flatten, *et al.*, *Scientific Reports* **6**, 33134 (2016).
104. V. G. Kravets, *et al.*, *Chemical Reviews* **118**, 5912 (2018).
105. J. Theiss, *et al.*, *Nano Letters* **10**, 2749 (2010).
106. Y. J. Liu, *et al.*, *Advanced Materials* **24**, OP131 (2012).
107. S. J. Tan, *et al.*, *Journal of Molecular and Engineering Materials* **2**, 1440011 (2014).
108. G. Si, *et al.*, *Nanoscale* **5**, 6243 (2013).
109. W. Zhou, *et al.*, *Nature Nanotechnology* **8**, 506 (2013).
110. M. De Giorgi, *et al.*, *ACS Photonics* **5**, 3666 (2018).
111. M. Ramezani, *et al.*, *Optica* **4**, 31 (2017).
112. B. Lee, *et al.*, *Nano Letters* **15**, 3646 (2015).
113. B. Lee, *et al.*, *Nano Letters* **17**, 4541 (2017).
114. S. Wang, *et al.*, *Nano Letters* **16**, 4368 (2016).
115. S. Wang, *et al.*, *ACS Photonics* **6**, 286 (2019).
116. L. Liu, *et al.*, *Advanced Optical Materials* (2019).
117. P. K. Jain, *et al.*, *The Journal of Physical Chemistry B* **110**, 7238 (2006).
118. M.-E. Kleemann, *et al.*, *Nature Communications* **8**, 1296 (2017).
119. X. Han, *et al.*, *ACS Photonics* **5**, 3970 (2018).
120. D. Zheng, *et al.*, *Nano Letters* **17**, 3809 (2017).
121. M. Wang, *et al.*, *Advanced Materials* **30**, 1705779 (2018).
122. M. Stuhrenberg, *et al.*, *Nano Letters* **18**, 5938 (2018).
123. J. Cuadra, *et al.*, *Nano Letters* **18**, 1777 (2018).
124. M. Geisler, *et al.*, *ACS Photonics* **6**, 994 (2019).
125. S. Hou, *et al.*, *Advanced Optical Materials* **7**, 1900857 (2019).
126. J. Sun, *et al.*, *ACS Nano* **12**, 10393 (2018).
127. Y. Yu, *et al.*, *Nano Letters* **17**, 3613 (2017).
128. V. G. Kravets, *et al.*, *npj 2D Materials and Applications* **3** (2019).
129. B. Chakraborty, *et al.*, *Nano Letters* **18**, 6455 (2018).
130. B. Munkhbat, *et al.*, *ACS nano* **14**, 1196 (2020).
131. P. Ni, *et al.*, *ACS Photonics* **6**, 1594 (2019).
132. S. Butun, *et al.*, *Nano Letters* **15**, 2700 (2015).
133. S. Butun, *et al.*, *ACS Applied Materials & Interfaces* **9**, 15044 (2017).
134. M.-G. Lee, *et al.*, *Nanoscale* **9**, 16244 (2017).
135. A. Sobhani, *et al.*, *Applied Physics Letters* **104**, 031112 (2014).
136. B. Mukherjee, E. Simsek, *Plasmonics* **11**, 285 (2016).
137. J. Lin, *et al.*, *Applied Physics Letters* **102**, 203109 (2013).
138. K. F. Mak, J. Shan, *Nature Photonics* **10**, 216 (2016).
139. E. M. Purcell, *et al.*, *Physical Review* **69**, 37 (1946).
140. W. Zhao, *et al.*, *Advanced Materials* **28**, 2709 (2016).
141. J. Kern, *et al.*, *ACS Photonics* **2**, 1260 (2015).
142. K. C. Lee, *et al.*, *Scientific Reports* **5**, 16374 (2015).
143. M. K. Schmidt, *et al.*, *Faraday Discussions* **205**, 31 (2017).
144. M. K. Schmidt, *et al.*, *ACS Nano* **10**, 6291 (2016).
145. W. Chen, *et al.*, *Light: Science & Applications* **7**, 56 (2018).
146. W. Zhu, K. B. Crozier, *Nature Communications* **5**, 5228 (2014).
147. J. Y. Kim, *et al.*, *Optics Express* **24**, 27546 (2016).
148. A. G. Milekhin, *et al.*, *Nanoscale* **10**, 2755 (2018).
149. S. A. Ghopry, *et al.*, *Advanced Optical Materials* **7**, 1801249 (2019).

150. M. Alamri, *et al.*, *ACS Applied Nano Materials* **2**, 1412 (2019).
151. E. Er, *et al.*, *Chemistry of Materials* **31**, 5725 (2019).
152. J. R. Schaibley, *et al.*, *Nature Reviews Materials* **1**, 16055 (2016).
153. N. Lundt, *et al.*, *2D Materials* **4**, 025096 (2017).
154. L. Sun, *et al.*, *Nature Photonics* **13**, 180 (2019).
155. B. Ding, *et al.*, *ACS Nano* **13**, 1333 (2019).
156. T. Chervy, *et al.*, *ACS Photonics* **5**, 1281 (2018).
157. G. Hu, *et al.*, *Nature Photonics* **13**, 467 (2019).
158. T. Wen, *et al.*, *Science Advances* **6**, eaao0019 (2020).
159. J. Echeverry, *et al.*, *Physical Review B* **93**, 121107 (2016).
160. Y. Zhou, *et al.*, *Nature Nanotechnology* **12**, 856 (2017).
161. K.-D. Park, *et al.*, *Nature Nanotechnology* **13**, 59 (2018).
162. M. Wang, *et al.*, *Small* **15**, 1900982 (2019).
163. M. Long, *et al.*, *Advanced Functional Materials* **29**, 1803807 (2019).
164. P. Berini, *Laser & Photonics Reviews* **8**, 197 (2014).
165. R. Kumar, *et al.*, *Advanced Optical Materials* **5**, 1700009 (2017).
166. Y. Liu, *et al.*, *Nature Communications* **2**, 579 (2011).
167. Z. Fang, *et al.*, *Nano Letters* **12**, 3808 (2012).
168. R. Chowdhury, *et al.*, *Nanoscale* **9**, 15591 (2017).
169. S. Bang, *et al.*, *Nano Letters* **18**, 2316 (2018).
170. Z.-Q. Wu, *et al.*, *Advanced Materials* **30**, 1706527 (2018).
171. B. Sun, *et al.*, *Advanced Functional Materials* **29**, 1900541 (2019).
172. N. Zhang, *et al.*, *Nanoscale* **6**, 1416 (2014).
173. Z. Cai, *et al.*, *The Journal of Physical Chemistry C* **117**, 9440 (2013).
174. N. Zhang, *et al.*, *Sensors and Actuators B: Chemical* **183**, 310 (2013).
175. L. Wu, *et al.*, *Optics Express* **18**, 14395 (2010).
176. P. K. Maharana, R. Jha, *Sensors and Actuators B: Chemical* **169**, 161 (2012).
177. Q. Ouyang, *et al.*, *Scientific Reports* **6**, 28190 (2016).
178. Q. Ouyang, *et al.*, *The Journal of Physical Chemistry C* **121**, 6282 (2017).
179. L. Wu, *et al.*, *Sensors and Actuators B: Chemical* **249**, 542 (2017).
180. X. Dai, *et al.*, *Sensors* **19**, 173 (2019).
181. L. Wu, *et al.*, *Journal of Lightwave Technology* **35**, 82 (2016).
182. Y. Feng, *et al.*, *Applied Optics* **57**, 3639 (2018).
183. J.-Y. Jing, *et al.*, *Optics and Lasers in Engineering* **112**, 103 (2019).
184. Y. Xu, *et al.*, *Journal of Physics D: Applied Physics* **52**, 065101 (2018).
185. L. Wu, *et al.*, *Plasmonics* **13**, 281 (2018).
186. H. Wang, *et al.*, *Photonics Research* **6**, 485 (2018).
187. N.-F. Chiu, *et al.*, *Nanoscale Research Letters* **9**, 445 (2014).
188. C. L. Holloway, *et al.*, *IEEE Antennas and Propagation Magazine* **54**, 10 (2012).
189. K. Sarabandi, N. Behdad, *IEEE Transactions on Antennas and propagation* **55**, 1239 (2007).
190. G. Si, *et al.*, *Applied Physics Letters* **99**, 033105 (2011).
191. F. Bayatpur, K. Sarabandi, *IEEE Transactions on Microwave Theory and Techniques* **56**, 774 (2008).
192. J. McVay, *et al.*, *IEEE Microwave and Wireless components letters* **14**, 130 (2004).
193. Z. Bayraktar, *et al.*, *IEEE Antennas and Wireless Propagation Letters* **10**, 1563 (2011).
194. F. Cheng, *et al.*, *Scientific Reports* **5**, 11045 (2015).
195. G. M. Akselrod, *et al.*, *Advanced Materials* **27**, 8028 (2015).
196. W. Zhu, *et al.*, *Applied Physics Letters* **108**, 121901 (2016).
197. M. Khorasaninejad, *et al.*, *Nano Letters* **17**, 1819 (2017).
198. N. Yu, *et al.*, *Science* **334**, 333 (2011).
199. X. Chen, *et al.*, *Nature Communications* **3**, 1 (2012).
200. H. Liu, *et al.*, *Nano Letters* **12**, 1549 (2012).

201. M. Mehmood, *et al.*, *Advanced Materials* **28**, 2533 (2016).
202. F. Qin, *et al.*, *Science Advances* **2**, e1501168 (2016).
203. M. Khorasaninejad, *et al.*, *Science* **352**, 1190 (2016).
204. A. Nemati, *et al.*, *Opto-Electronic Advances* **1**, 180009 (2018).
205. J. Lee, *et al.*, *Advanced Optical Materials* **2**, 1057 (2014).
206. A. Nemati, *et al.*, *Journal of Optics* **21**, 055102 (2019).
207. P. Gutruf, *et al.*, *ACS Nano* **10**, 133 (2016).
208. P. C. Wu, *et al.*, *Nature Communications* **10**, 1 (2019).
209. G. Kafaie Shirmanesh, *et al.*, *Nano Letters* **18**, 2957 (2018).
210. A. She, *et al.*, *Science Advances* **4**, eaap9957 (2018).
211. H.-S. Ee, R. Agarwal, *Nano Letters* **16**, 2818 (2016).
212. F. Wang, *et al.*, *Science* **320**, 206 (2008).
213. S. H. Lee, *et al.*, *Nature Materials* **11**, 936 (2012).
214. Y. Yao, *et al.*, *Nano Letters* **14**, 6526 (2014).
215. N. Dabidian, *et al.*, *ACS Photonics* **2**, 216 (2015).
216. M. M. Jadidi, *et al.*, *Nano Letters* **15**, 7099 (2015).
217. P. Q. Liu, *et al.*, *Nature Communications* **6**, 1 (2015).
218. J. Li, *et al.*, *Advanced Optical Materials* **4**, 91 (2016).
219. H. Yan, *et al.*, *Nature Nanotechnology* **7**, 330 (2012).
220. N. Papasimakis, *et al.*, *Light: Science & Applications* **2**, e78 (2013).
221. Y. Fan, *et al.*, *ACS Photonics* **2**, 151 (2015).
222. A. Kumar, *et al.*, *Nano Letters* **15**, 3172 (2015).
223. M. A. Othman, *et al.*, *Optics Express* **21**, 7614 (2013).
224. C. E. Petoukhoff, *et al.*, *ACS Nano* **10**, 9899 (2016).
225. P. Grangier, *et al.*, *Scalable Quantum Computers* pp. 89–104 (2001).
226. J. Gu, *et al.*, *arXiv preprint arXiv:1905.12227* (2019).
227. R. P. Puchert, *et al.*, *Nature Nanotechnology* **12**, 637 (2017).
228. R. F. Oulton, *et al.*, *Nature* **461**, 629 (2009).
229. E. Y. Paik, *et al.*, *Nature* **576**, 80 (2019).
230. Y. Liu, *et al.*, *Science Advances* **5**, eaav4506 (2019).
231. R.-M. Ma, *et al.*, *Nature Nanotechnology* **9**, 600 (2014).